Available online at www.sciencedirect.com

ScienceDirect

Procedia CIRP 108 (2022) 37–42

www.elsevier.com/locate/procedia

6th CIRP Conference on Surface Integrity

Influence of Surface Integrity and Coating on the High Cycle Fatigue Properties of 300M Steel from Self-Heating Tests under Cyclic Loads

P. LEPITRE[a,b,*], S. CALLOCH[a], C. DOUDARD[a], M. DHONDT[a], M. SURAND[b]

[a]*École Nationale Supérieure des Techniques Avancées, ENSTA Bretagne, UMR CNRS 6027, IRDL, 2 Rue François Verny, 29200 Brest, France*
[b]*Safran Landing Systems, 7 Rue Général Valérie André, 78140 Vélizy-Villacoublay, France*

* Corresponding author. Tel.: +33 6 74 72 07 96. *E-mail address:* pierrick.lepitre@ensta-bretagne.org

Abstract

300M, an ultra-high strength steel used in aeronautics for landing gears, is generally shot-peened and coated with High Velocity Oxygen Fuel sprayed WC-10Co-4Cr to improve tribological behavior. In literature, few treatment parameters have been tested to analyze the surface integrity influence on fatigue properties. The self-heating method under cyclic loading is used to quickly determine fatigue properties by coupling them with intrinsic dissipation. Investigations on dissipation mechanisms of coating and substrate enable to develop self-heating models. That is the first step to build a lifespan forecast model based on temperature measurement to study shot-peening and coating influence on fatigue properties.

Keywords: HVOF Coating; Shot-Peening; Fatigue

1. Introduction

Determining a full S/N curve is a fastidious, time consuming, and expensive task, primarily due to the high number of cycles and the resulting data scatter. Furthermore, due to the fact that numerous parameters have an influence on fatigue properties, it is impractical to obtain fatigue curves for every configuration. Consequently, it is common practice to carefully select some sets of parameters to be tested and subsequently determine fatigue abatement factors for untested configurations. This approach leads to time consuming and expensive characterization test campaigns. The scientific and industrial community have both worked towards finding new methods for determining fatigue properties that would improve the current situation. One such approach, named “self-heating”, utilizes temperature measurements to forecast fatigue properties. In 1914, Stromeyer [1] noticed that under cyclic loading, steels dissipate energy thus self-heat. He demonstrated that the temperature rise increases abruptly when the loading amplitude exceeds a threshold, and he was able to demonstrate good correlation between this threshold and the material’s fatigue limit. Following this work, self-heating under cyclic loading method has been applied with various degrees of success for steel grades [2,3,4,5], other metal alloys [6,7], as well as for composites and rubbers [8,9,10]. If an empirical approach can provide great estimation of the fatigue limit, the self-heating method may provide additional information, such as the dispersion of properties or fatigue life. Models are then required; dissipation mechanisms must be understood and modeled to establish links with fatigue mechanisms. This kind of approach has been demonstrated and validated for various steel grades [3,11].

The “self-heating under cyclic loadings method” consists of applying blocks of cyclic loadings at increasing stress amplitudes (figure 1.a) and measuring the temperature rise after stabilization (figure 1.b). By measuring temperature at a much lower frequency than the loading frequency, the global contribution of the thermoelastic coupling is null and so only the intrinsic heat dissipation of the material participates to the temperature rise [4]. By solving the heat equation, the temperature can be directly correlated to the intrinsic heat dissipation of the material. If the heat dissipation mechanisms

10.1016/j.procir.2022.03.012

are linked to fatigue mechanisms, the calculation of heat dissipation can provide information on the fatigue properties.

The aim of this study is to apply the self-heating method to an ultra-high tensile strength steel (300M) with specific surface treatment (shot-peened, grit-blasted and coated with thermally sprayed WC-CoCr powders) to develop a forecast lifespan model.

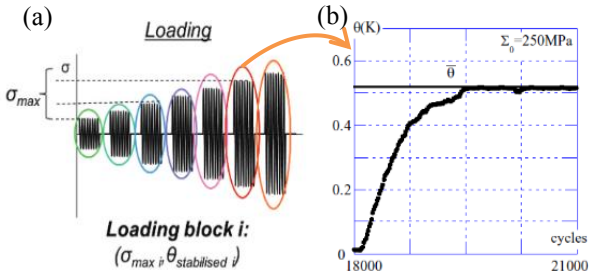

Fig. 1. Loading procedure (a)
and temperature evolution during a loading block (b)

Nomenclature

T_1: Top jaw temperature
T_2: Test coupon temperature
T_3: Bottom jaw temperature
θ: Temperature rise
ρ: Specific mass
c: Specific heat capacity
f_r: Loading frequency
σ_a: Loading amplitude
σ_D: Fatigue limit at 10^6 cycles, R = -1
τ_{eq}: Equivalent time corresponding to the thermal loses
S_i, i∈ {B, SP, GB, Int, C}: Heat source term for the i zone
$E_{d,\,i}$, i∈ {bare, SP, HVOF, HVOF-2, stripped}: Mean intrinsic dissipation of the i configuration

2. Background

300M is a low-alloy steel (composition according to AMS6257F [12]). With a minimum tensile strength of 1930 MPa and a minimum 0.2 % offset yield strength of 1586 MPa [12], 300M is categorized as an ultra-high tensile strength (UHTS) steel. Combined with a good toughness ($K_{IC} \approx 60$ MPa.m$^{1/2}$) [13,14] and good fatigue properties ($\sigma_D \approx 830$ MPa) [2,14], 300M is used in aerospace for landing gears to achieve safety, weight, and size requirements [15]. To prevent wear and corrosion, surface treatments have to be applied. When wear resistance is required, hard chrome plating was historically used but, due to environmental and health issues [16], it is being replaced by tungsten carbide-based coatings. In recent years, a WC-CoCr coating applied by High Velocity Oxygen Fuel (HVOF) fulfills this role [17,18,19] thanks to its high hardness ($H_v > 1\,000$) [20]. By burning fuel, gas is heated up to 3000 °C and accelerated up to 2000 m.s^{-1} [21] before the WC-CoCr powder is inserted. Enough energy has to be transferred to the powder to melt the CoCr matrix and to ensure good adhesion between the substrate and the coating. The elastic and thermal properties mismatch and the powder effects adversely affect material fatigue life [14,22,23]. In order to reduce these and to increase the substrate-coating bond by creating a favorable surface condition, 300M is shot-peened and then grit-blasted prior to coating.

Due to this surface treatment, the intrinsic dissipation is not homogenous anymore. However only an average value of the intrinsic heat dissipation can be determined with the self-heating method. If it is considered that each operation of the coating process affects the dissipation on a local area, five regions with their own dissipation level can be considered: the bulk (S_B), the shot-peening affected zone (S_{SP}), the grit-blasting affected zone (S_{GB}), the coating-substrate interphase (S_{Int}), and the coating (S_C). This configuration (HVOF) can be depicted in figure 2.a; a cross-section view with the intrinsic dissipation of each zone is shown by a red line. To compare results, a bare 300M steel test coupon without any surface treatment (bare configuration) is considered (figure 2.b).

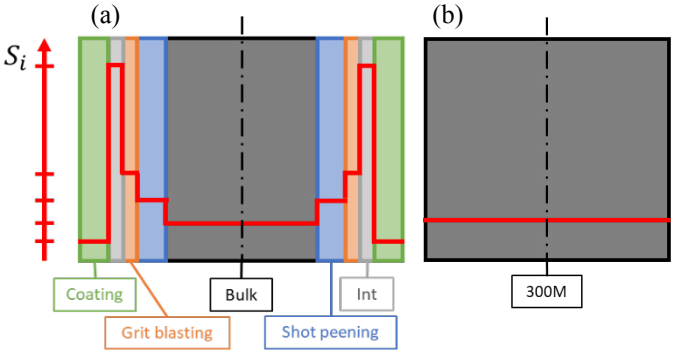

Fig. 2. Cut view of an HVOF (a) and bare (b) configuration test coupon with the different regions and their dissipation levels.

3. Experimental

3.1. Instrumentation and protocol

To conduct self-heating tests, a Zwick Vibrophore Amsler 50 kN machine was used. The tests were conducted in load control with a load ratio of -1 and a loading frequency of $f_r = 135$ Hz on cylindrical unnotched test coupons, $K_t = 1$, with a 50 mm² section. The test coupon temperature (T_2) was recorded by a K-type thermocouple. The temperature of the two clamping parts of the test machine were also recorded (T_1 and T_3) to prevent environment influence. An example of temperatures evolutions is shown in figure 3.a. The temperature rise is defined as the difference between the test coupon temperature and the mean temperature of the clamping parts (figure 3.b),

$$\theta = T_2 - (T_1 + T_3)/2 \quad (1)$$

Moreover, the temperature rise curve is shifted to suppress its average component before the test beginning. The stabilized temperature rise is recorded after 35 000 cycles (4min 20s for 135 Hz). Subsequently, the test is paused for a minimum of 5 minutes to allow the coupon to cool down to the ambient temperature. This procedure is applied for ascending loading amplitude on the same test coupon until failure. The loading amplitude / stabilized temperature rise graph is called a self-heating curve. Thanks to a 0D resolution of the heat equation [11], the dissipated energy can be calculated with the temperature rise, τ_{eq} being determined with the decay part of the temperature rise curves:

$$E_d = \theta * \rho c / (fr * \tau_{eq}) \quad (2)$$

As the τ_{eq} can change between tests, results will be expressed by dissipated energy. Absolute levels of dissipation cannot be directly interpreted, only regime changes and comparison between configurations can be.

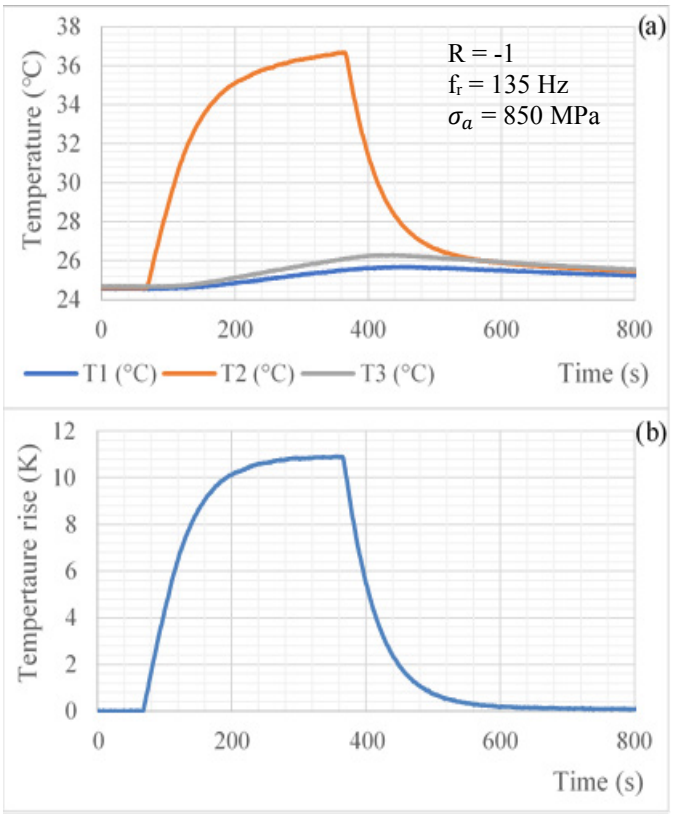

Fig. 3. Test coupon and clamping parts temperatures (a) and temperature rise evolution (b) for an HVOF configuration

3.2. First self-heating results

Figure 4.a shows the self-heating curves of bare and HVOF configurations. The bare test coupon did not fracture while the HVOF test coupon fractured at σ_a = 900 MPa. To distinguish the two self-heating regimes, self-heating curves can be plotted in logarithm graphs (figure 4.b). As shown by previous studies [3,24,25], the first regime of steel has a constant slope around 2 in log-log graph. In our tests, 300M even with a WC-CoCr coating, seems to follow a similar slope, with a 2-slope for the bare configuration and 2.2 for the HVOF configuration (straight lines in transparency, figure 4.b). The second regime is characterized by an increase of the slope. The HVOF test coupon fractured before the beginning of the 2nd regime while only few points for the bare configuration have been measured. The determinist self-heating model of Doudard [11] gives a first value for the 300M fatigue limit of $\sigma_D \approx$ 850 MPa. For the HVOF configuration, such analysis cannot be made because of the heterogeneity of the configuration and the stabilized temperature rise measured, which means that the dissipated energy is only an average of different contributions. Nevertheless, the great difference between the bare and the HVOF configuration dissipation is an indication of new dissipation mechanisms implied by the surface treatments and the coating.

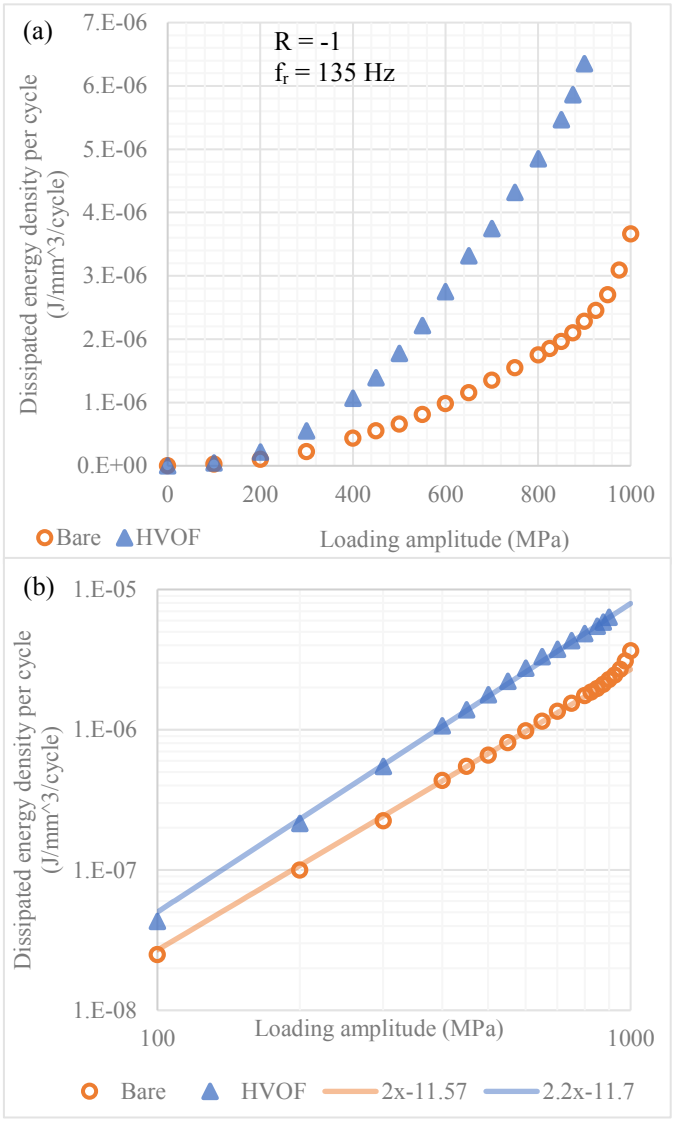

Fig. 4. Intrinsic dissipation of bare and HVOF configurations in a linear diagram (a) and in a logarithm diagram (b)

4. Results and discussions

4.1. Comprehension model

To decompose the average thermal signal of the HVOF configuration, the dissipation of middle configurations can be studied. The reference configuration is a test coupon made of 300M bare material (without any surface treatments), previously called the bare configuration (figure 5.a). A typical configuration to consider is a shot-peened test coupon (SP configuration, figure 5.b). Aside from the HVOF configuration (figure 5.c), another coated configuration was also considered. The second HVOF (HVOF-2) method consists on a removal of the grit-basting and a reduction of the coating thickness. So, an HVOF-2 configuration presents a bulk, a shot-peening affected zone, a coating-substrate interphase and a coating (figure 5.d). The last studied configuration is based on an HVOF test coupon from which the coating has been stripped by electro-chemical method [26]. A stripped HVOF configuration presents a bulk, a shot-peening affected zone, a grit-blasting affected zone and the 300M part of the coating-substrate interphase (figure 5.e).

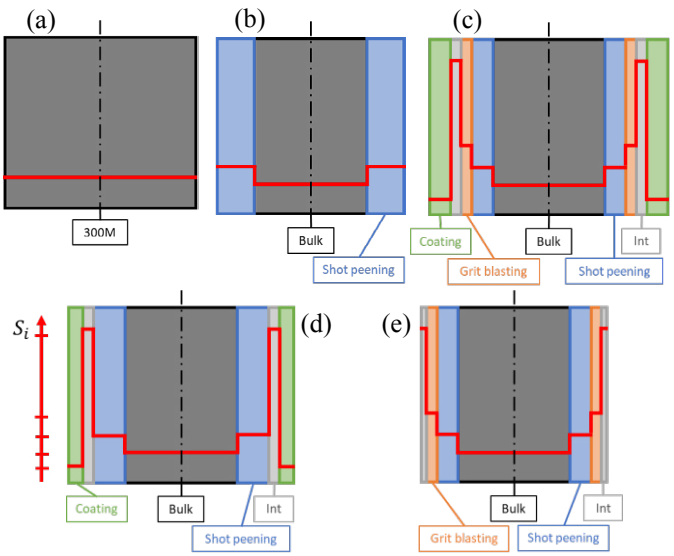

Fig. 5. Cut view of a bare (a), SP (b), HVOF (c), HVOF-2 (d) and HVOF-stripped (e) configuration test coupon with their dissipation levels

4.2. Self-heating results

For each configuration, the self-heating curve has been determined with a single test coupon with the experimental protocol explained in paragraph 3.1 (figure 6.a and 6.b). Both the HVOF and HVOF-2 test coupons fractured at $\sigma_a = 900$ MPa and the bare, SP and HVOF-stripped test coupons reached the machine limits without fracture. It can be observed that the HVOF-stripped configuration dissipates exactly as the bare configuration, whereas the self-heating method can distinguish the SP and the bare configurations. The SP configuration first regime seems to follow a 2.2-slope and the transition between the first and the second regime seem to occur earlier (900 MPa instead of 950 MPa). With regards to the HVOF-2 configuration, it seems to dissipate similarly to the HVOF configuration; the 2.2-slope of the first regime is generally respected although more dispersion is noticeable.

4.3. Intrinsic dissipation estimation

To estimate the heat dissipation of each zone, calculation of each region's volume is required. As the test coupons are axisymmetric and the temperature can be considered homogenous in the gauge length, only the radius is varied. The nominal radius of a test coupon is 3.99 mm, the shot-peened affected zone is considered to be 150 µm deep, the grit-blasted zone is considered to be 50 µm deep and the coating-substrate interphase 50 µm thick (25 µm for 300M; 25 µm for coating). Those thickness values were chosen based on literature [14, 27] and fracture surface observations. For the HVOF configuration, the coating thickness is 150 µm and for HVOF-2, 80 µm. The calculations were made for $\sigma_a = 900$ MPa.

For the bare configuration, the test coupon dissipation can be considered homogenous and so the bulk dissipation in other configurations should be

$$E_{d,bare} = S_B = 2.28\ \mu J.mm^{-3}.cycle^{-1} \quad (3)$$

For the shot-peened configuration,

$$E_{d,SP} = \frac{S_B * V_B + S_{SP} * V_{SP}}{V_B + V_{SP}} = 2.76\ \mu J.mm^{-3}.cycle^{-1} \quad (4)$$

so $S_{SP} = 8{,}79\ \mu J.mm^{-3}.cycle^{-1}$.

For the HVOF and HVOF-2 configurations, the coating thickness seems not to affect the dissipation:

- $E_{d,HVOF} = 6.35\ \mu J.mm^{-3}.cycle^{-1}$;
- $E_{d,HVOF-2} = 6.32\ \mu J.mm^{-3}.cycle^{-1}$.

The coating should not dissipate significantly compared to the bulk, so $S_C \approx 0\ J.mm^{-3}.cycle^{-1}$. Moreover, the grit-blasting seems not to affect the dissipation level, therefore we can assume that $S_{GB} \approx S_{SP} = 8{,}79\ \mu J.mm^{-3}.cycle^{-1}$.

For the HVOF-stripped configuration, we calculate $E_{d,stripped} = 2.24\ \mu J.mm^{-3}.cycle^{-1} \approx E_{d,bare}$. The electro-chemical stripping process does not attack the substrate and, therefore, should not influence the bulk, shot-peening affected zone, and grit-blasting affected zone dissipation. However, the HVOF-stripped configuration dissipates equally to the bare configuration, suggesting that the HVOF process nullifies the shot-peening and grit-blasting effects and does not induce dissipation in the coating-substrate interphase. Dissipation of coated configuration would then come from interactions between substrate and coating. Thus, the different configurations can be simplified (figure 7).

$$E_{d,HVOF} = \frac{S_B * (V_B + V_{SP} + V_{GB}) + S_{Int} * V_{Int}}{V_B + V_{SP} + V_{GB} + V_{Int} + V_C} = 6.35\ \mu J.mm^{-3}.cycle^{-1} \quad (5)$$

so $S_{Int} = 183\ \mu J.mm^{-3}.cycle^{-1}$.

All configuration mean dissipations can be seen in table 1 and the calculated dissipations in table 2.

4.4. Discussion

All self-heating results have been obtained from one test coupon per configuration, except for the bare configuration. Therefore, further testing to produce additional results is required. Nevertheless, for the bare configuration, results have shown good repeatability. In addition, the test coupons of each configuration have to be characterized to validate the model hypothesis e.g. affected zone thicknesses, impact of each process etc. Stress profile and microhardness profiles are planned along with composition and microstructure maps.

Moreover, new configuration should be tested (such as grit-blasted configuration) and different test coupon geometry can be used. One suggestion is using a sandwich test coupon (surface treatments and coatings applied on two faces of a rectangular test coupon) which allows for the cross-section to be observed. With an IR camera, the temperature along the thickness can be measured, thus the heat source term can be determined along the thickness and the dissipation of each zone can be calculated. Besides, a direct view of each zone will help to propose and validate dissipation mechanisms for each zone and to link them with fatigue mechanisms to build a forecast lifespan model for 300M coated configuration.

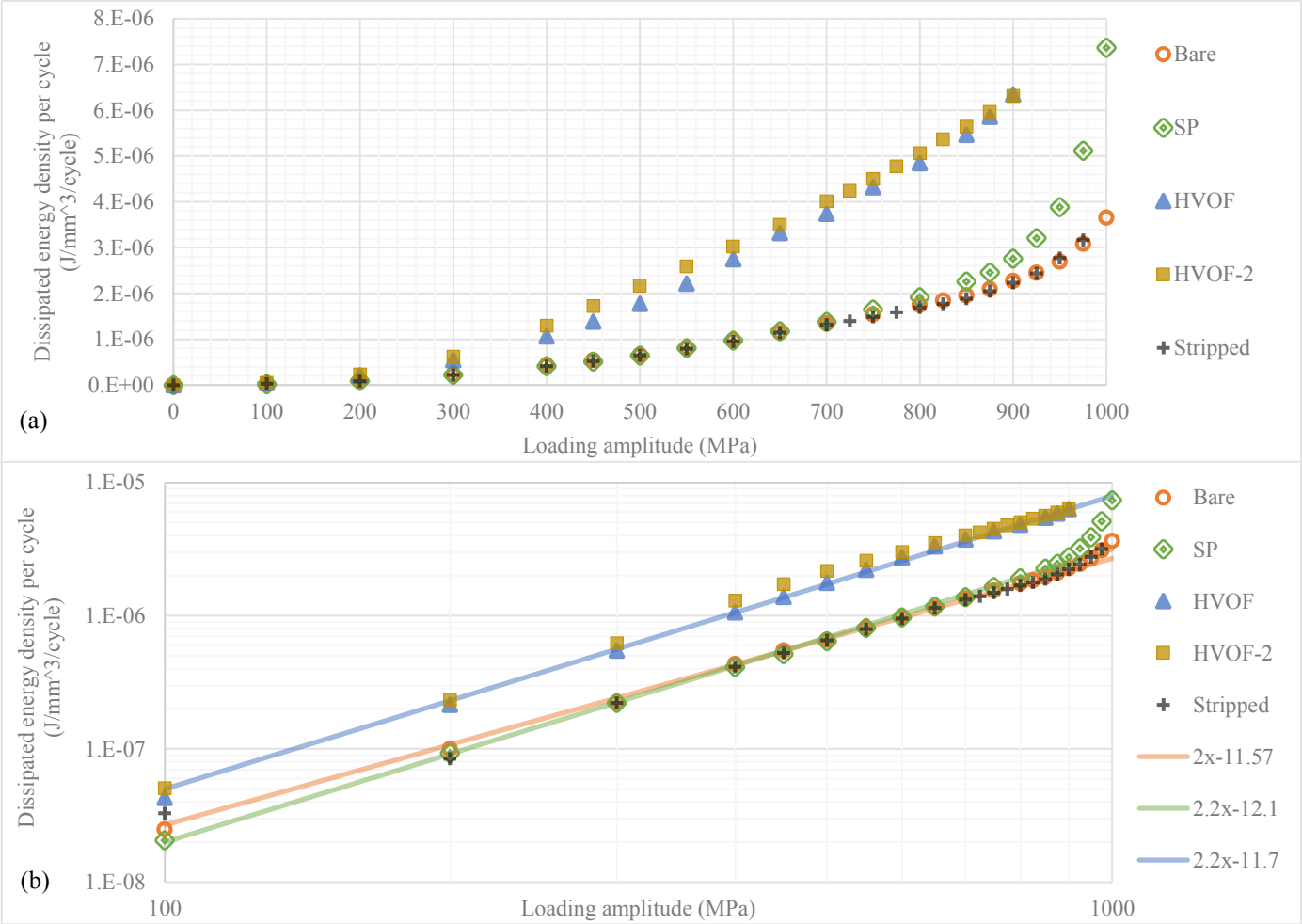

Fig. 6. Intrinsic dissipation of bare, SP, HVOF, HVOF-2 and HVOF-stripped configurations in a linear diagram (a) and in a logarithm diagram (b)

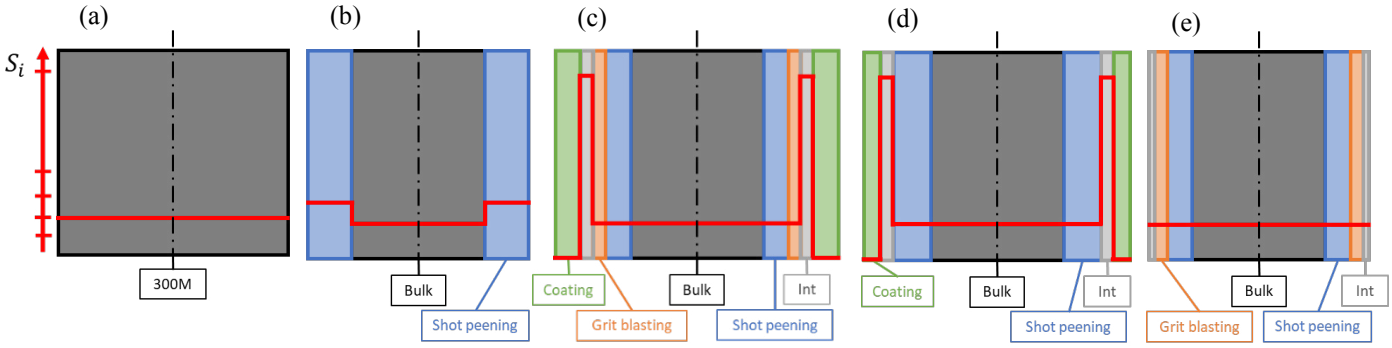

Fig 7. Cut view of a bare (a), SP (b), HVOF (c), HVOF-2 (d) and HVOF-stripped (e) configuration test coupon with their simplified dissipation levels

Table 1. Configuration mean dissipation levels for $\sigma_a = 900$ MPa

Configuration	Bare	Shot-peened	HVOF	HVOF-2	HVOF-stripped
Dissipation ($\mu J.mm^{-3}.cycle^{-1}$)	2.28	2.76	6.35	6.32	2.24

Table 2. Zone dissipation levels for $\sigma_a = 900$ MPa

Zone	Bulk	Shot-peening affected zone	Grit-blasting affected zone	Coating-substrate interphase	Coating
Dissipation ($\mu J.mm^{-3}.cycle^{-1}$)	2.28 (ref.)	8.79 (x 4)	8.79 (x 4)	183 (x 80)	0

5. Conclusion

Self-heating curves of bare 300M steel and coated 300M steel with HVOF sprayed WC-CoCr powder have been determined. Due to test machine limitations, only the first regime with few points in the second regime have been measured. The determinist self-heating model of Doudard [11], provides a first estimation of the fatigue limit at $\sigma_D \approx 850$ MPa for the bare configuration, which is close to the commonly accepted fatigue limit ($\sigma_D \approx 830$ MPa [14,15]). As the HVOF configuration is highly heterogeneous, such model cannot be

applied and the temperature only allows for an estimation of the mean dissipation of the whole test coupon.

A simple model has been devised to distinguish the contribution of each zone. The model considers that every surface treatment has an impact on dissipation level of a layer of the test coupon. Five zones have been identified, the bulk (300M), the shot-peening affected zone, the grit-blasting zone, the coating-substrate interphase (affected by the HVOF process but also where the interactions between the substrate and the coating occurs) and the HVOF coating zone. To determine dissipation of each zone, intermediate configurations have been tested: a shot-peened test coupon, an HVOF-2 coupon (coating process without grit-blasting and smaller coating thickness) and an HVOF-stripped test coupon (an HVOF sprayed coupon with subsequent electro-chemical removal).

Thanks to the clear effect of each operation of the coating process on intrinsic dissipation, self-heating method can be easily applied to each zone. Shot-peening has a clear effect on dissipation level of the shot-peening affected zone (x4 compared to reference configuration). The HVOF and HVOF-2 configuration dissipate approximately the same amount of energy, whereas the grit-blasting seems not to impact the dissipation of a shot-peened test coupon and the coating seems not to dissipate significantly compared to other zones. In conclusion, the substantial dissipation increase of coated configurations comes from the coating-substrate interphase. As the HVOF-stripped configuration dissipates similarly to the bare configuration, the HVOF process seems to be suppressing the shot-peening effect on dissipation. Thus, the comprehension model can be simplified by considering a 300M zone (the bulk), a coating zone (without dissipation) and a coating-substrate interphase where most of the dissipation occurs. To validate the results and test the hypothesis, each configuration has to be characterized.

Acknowledgement

This work has been carried out within the frame of the Self-Heating industrial chair co-funded by Safran, Naval Group and the French National Agency for Research (ANR).

References

[1] Stromeyer, C.E., 1914. The determination of fatigue limits under alternating stress conditions. Proc. R. Soc. Lond. A 90, 411–425.

[2] Xue, H., Liu, P., Chen, P., Wang, J., 2012. Fatigue life assessment of a high strength steel 300 M in the gigacycle regime. Theoretical and Applied Mechanics Letters 2, 031006.

[3] Munier, R., Doudard, C., Calloch, S., Weber, B., 2014. Determination of high cycle fatigue properties of a wide range of steel sheet grades from self-heating measurements. International Journal of Fatigue 63, 46–61.

[4] Doudard, C., Calloch, S., Cugy, P., Galtier, A., Hild, F., 2005. A probabilistic two-scale model for high-cycle fatigue life predictions. Fat Frac Eng Mat Struct 28, 279–288.

[5] De Finis, R., Palumbo, D., Ancona, F., Galietti, U., 2015. Fatigue limit evaluation of various martensitic stainless steels with new robust thermographic data analysis. International Journal of Fatigue 74, 88–96.

[6] Roué, V., Doudard, C., Calloch, S., Montel, F., Pujol D'Andrebo, Q., Corpace, F., 2018. Rapid determination of the high cycle fatigue properties of high temperature aeronautical alloys by self-heating measurements. MATEC Web Conf. 165, 22022.

[7] Ezanno, A., Doudard, C., Calloch, S., Millot, T., Heuzé, J.-L., 2010. Fast characterization of high-cycle fatigue properties of a cast copper–aluminum alloy by self-heating measurements under cyclic loadings. Procedia Engineering 2, 967–976.

[8] Le Saux, V., Marco, Y., Calloch, S., Doudard, C., Charrier, P., 2010. Fast evaluation of the fatigue lifetime of rubber-like materials based on a heat build-up protocol and micro-tomography measurements. International Journal of Fatigue 32, 1582–1590.

[9] Jegou, L., Marco, Y., Le Saux, V., Calloch, S., 2013. Fast prediction of the Wöhler curve from heat build-up measurements on Short Fiber Reinforced Plastic. International Journal of Fatigue 47, 259–267.

[10] Peyrac, C., Jolliviet, T., Leray, N., Lefebvre, F., Westphal, O., Gornet, L., 2015. Self-heating Method for Fatigue Limit Determination on Thermoplastic Composites. Procedia Engineering 133, 129–135.

[11] Luong, M.P., 1998. Fatigue limit evaluation of metals using an infrared thermographic technique. Mechanics of Materials 28, 155–163.

[12] Aerospace Material Specification, 2016. Steel Bars, Forgings, and Tubing 1.6Si - 0.82Cr - 1.8Ni - 0.40Mo - 0.08V (0.40 - 0.44C) Consumable Electrode Vacuum Remelted Normalized and Tempered (AMS6257F

[13] Youngblood, J.L., Raghavan, M., 1977. Correlation of microstructure with mechanical properties of 300m steel. Metallurgical Transactions A 8, 1439–1448.

[14] Bag, A., 2019. Effect of shot peening on the axial fatigue life of 300M steel (Génie mécanique). Polytechnique Montréal, Montréal.

[15] Tomita, Y., 2000. Development of fracture toughness of ultrahigh strength, medium carbon, low alloy steels for aerospace applications. International Materials Reviews 45, 27–37.

[16] Sartwell, B.D., Legg, K.O., Schell, J., Sauer, J., Natishan, P., Dull, D., Falkowski, J., Bretz, P., Devereaux, J., Edwards, C., Parker, D., 2004. Validation of HVOF WC/Co Thermal Spray Coatings as a Replacement for Hard Chrome Plating on Aircraft Landing Gear. Naval Research Laboratory 275.

[17] Ko, P.L., Robertson, M.F., 2002. Wear characteristics of electrolytic hard chrome and thermal sprayed WC–10 Co–4 Cr coatings sliding against Al–Ni–bronze in air at 21 °C and at −40 °C. Wear 252, 880–893.

[18] Bolelli, G., Giovanardi, R., Lusvarghi, L., Manfredini, T., 2006. Corrosion resistance of HVOF-sprayed coatings for hard chrome replacement. Corrosion Science 48, 3375–3397.

[19] Verdon, C., Karimi, A., Martin, J.-L., 1998. A study of high velocity oxy-fuel thermally sprayed tungsten carbide based coatings. Part 1: Microstructures. Materials Science and Engineering: A 246, 11–24.

[20] Jacobs, L., Hyland, M.M., De Bonte, M., 1999. Study of the Influence of Microstructural Properties on the Sliding-Wear Behavior of HVOF and HVAF Sprayed WC-Cermet Coatings. Journal of Thermal Spray Technology 8, 125–132.

[21] Weman, K., 2012. Surface cladding and hardfacing methods, in: Welding Processes Handbook. Elsevier, pp. 151–156.

[22] Voorwald, H.J.C., Souza, R.C., Pigatin, W.L., Cioffi, M.O.H., 2005. Evaluation of WC–17Co and WC–10Co–4Cr thermal spray coatings by HVOF on the fatigue and corrosion strength of AISI 4340 steel. Surface and Coatings Technology 190, 155–164.

[23] Vackel, A., Sampath, S., 2017. Fatigue behavior of thermal sprayed WC-CoCr- steel systems: Role of process and deposition parameters. Surface and Coatings Technology 315, 408–416.

[24] Mareau, C., Favier, V., Weber, B., Galtier, A., Berveiller, M., 2012. Micromechanical modeling of the interactions between the microstructure and the dissipative deformation mechanisms in steels under cyclic loading. International Journal of Plasticity 32–33, 106–120.

[25] Curà, F., Gallinatti, A.E. and Sesana, R. (2012), Dissipative aspects in thermographic methods. Fatigue & Fracture of Engineering Materials & Structures, 35: 1133-1147.

[26] Aerospace Material Specification (2016). Chemical Check Analysis Limits Wrought Heat and Corrosion Resistant Steels (AMS2248H). SAE International.

[27] Gui, M., Eybel, R., Asselin, B., Monerie-Moulin, F., 2015. Cracking and Spalling Behavior of HVOF Thermally Sprayed WC-Co-Cr Coating in Bend and Axial Fatigue Tests. J. of Materi Eng and Perform 24, 1347-1356.